Ultrafast Photoconversion of the Green Fluorescent Protein Studied by Accumulative Femtosecond Spectroscopy

Florian Langhojer,[†‡] Frank Dimler,[†‡] Gregor Jung,[§] and Tobias Brixner[†‡*]
[†]Institut für Physikalische Chemie, Universität Würzburg, Am Hubland, 97074 Würzburg, Germany; [‡]Physikalisches Institut, Universität Würzburg, Am Hubland, 97074 Würzburg, Germany; and [§]Biophysikalische Chemie, Universität des Saarlandes, 66123 Saarbrücken, Germany

ABSTRACT The irreversible photoconversion of T203V green fluorescent protein (GFP) via decarboxylation is studied under femtosecond excitation using an accumulative product detection method that allows us to measure small conversion efficiencies of down to $\Delta OD = 10^{-7}$ absorbance change per pulse. Power studies with 800- and 400-nm pulse excitation reveal that excitation to higher states of the neutral form of the GFP chromophore induces photoconversion very efficiently. The singly excited neutral chromophore is a resonant intermediate of the two-step excitation process that leads to efficient photoconversion. We determine the dynamics of this two-step process by separating the excitation step of the neutral chromophore from the further excitation step to the reactive state in a time-resolved two-color experiment. The dynamics show that a further excitation to the very reactive higher excited state is only possible from the initially excited neutral chromophore and not from the fluorescent intermediate state. For applications of GFP in two-photon fluorescence microscopy, the found photochemical behavior implies that the high intensity conditions used in microscopy can lead to photoconversion easily and care has to be taken to avoid unwanted photoconversion.

INTRODUCTION

In the past two decades, fluorescence became the basis for many standard analytical tools in the life sciences due to its detection sensitivity and specificity toward analytes. The availability of compact and powerful laser sources triggered the development of new fluorophores and of detection schemes beyond ordinary luminescence excitation. Manipulating intervention into the emission process by stimulated emission was applied to localize cellular structures with unprecedented accuracy in optical microscopy (1). Photoactivation was used to map proteins with temporal and spatial resolution (2). The first method repetitively exploits the cyclic population of different photophysical states of a dye molecule, whereas the latter technique is based on irreversible phototransformations (3,4). Autofluorescent proteins, especially, apply as effector molecules for this purpose.

The best-known representative among the autofluorescent proteins is green fluorescent protein (GFP) from the pacific jellyfish *Aequorea victoria*. Shortly after the experimental proof that its fluorescence can be encoded genetically (5), it was shown that GFP exhibits an excited state proton-transfer reaction upon excitation with $\lambda \approx 400$ nm; the photocycle of the Thr^{203}Val (T203V) mutant is shown in Fig. 1 and spectra in Fig. 2. Herein, the neutral chromophore state RH releases a proton to the protein matrix leaving a deprotonated, metastable anionic chromophore state, R_I^-* (6–9). After photon emission at 510 nm, this intermediate state in the photocycle of GFP undergoes reprotonation within <1 ns (10). It could be stabilized by site-directed mutagenesis (11). In addition to R_I^-, a stable, equilibrated anionic chromophore state R_{eq}^- exists in wild-type (wt)-GFP, which absorbs at ~480 nm and fluoresces at ~510 nm. Although for different mutants these two absorptions of wt-GFP at ~400 nm and ~480 nm are shifted in wavelength and of different strength, one finds both absorption maxima (usually denoted as A and B forms) in most GFP mutants. In addition to these reversibly interconverting chromophore species, prolonged irradiation of the protein causes photoconversion, by which an anionic chromophore state R_{pc}^- (Fig. 1, *right*)—also with green fluorescence—is created. The reaction pathway was previously not considered to proceed via a doubly excited state RH** as shown in Fig. 1; this mechanism is one of the main results of this work as discussed below. The optical properties of the converted form are very similar to those of R_{eq}^-, the B form; for T203V GFP, absorption and fluorescence of R_{pc}^- occurs at 500 nm and 510 nm, respectively. Crystallography, mass spectrometry, optical, and vibrational spectroscopy were used to unravel the underlying structural rearrangements. It turned out that this irreversible phototransformation is characterized by decarboxylation of Glu^{222}, which is in close contact to the chromophore (12–14).

In previous studies (12–15), a strong dependence of the photoconversion of GFP on the excitation wavelength was found; ultraviolet (UV) light proved to be more efficient at inducing photoconversion than visible light. Additionally, a Kolbe-type mechanism was suggested to be responsible for the photoconversion, starting with an excited chromophore that accepts an electron from the Glu^{222} rest which, in turn, is decarboxylated. Therefore, the efficiency of UV light is explained by the higher oxidizing power of excited chromophore states higher than RH*. Although that study

Submitted September 10, 2008, and accepted for publication November 24, 2008.

*Correspondence: brixner@phys-chemie.uni-wuerzburg.de

Editor: Alberto Diaspro.

0006-3495/09/04/2763/8 $2.00

doi: 10.1016/j.bpj.2008.11.049

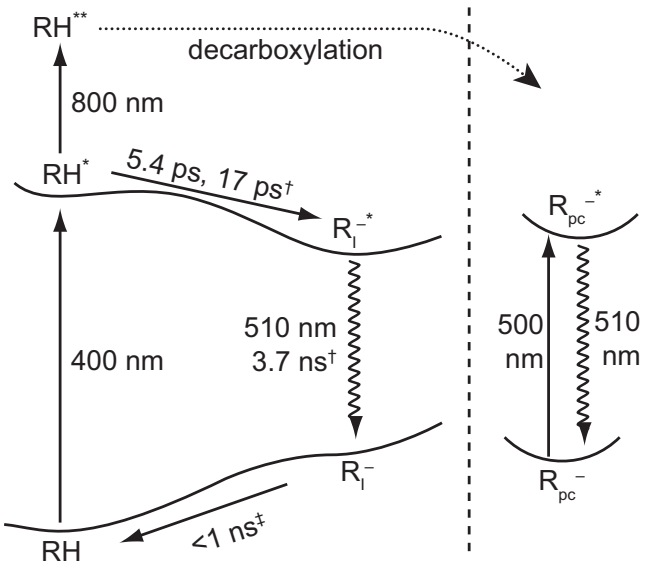

FIGURE 1 Simple potential energy scheme of T203V GFP. (*Left*) Photocycle of the RH form of GFP including excitation, excited state proton transfer, fluorescence, and reprotonation. In this study, it was found that further excitation from RH* with 800 nm leads to a higher excited state RH**, which is responsible for decarboxylation under femtosecond excitation conditions (*dotted arrow*). Time constants (†,‡) taken from the literature (10,17). (*Right*) Photoconverted form R_{pc}^-.

was performed under continuous-wave (CW) conditions and the role of RH* in the photoconversion process remains ambiguous (14), a major part of modern studies involving GFP use picosecond or femtosecond radiation for excitation, e.g., two-photon absorption (TPA) microscopy. The transient molecular species in combination with possible multiphoton absorptions constitute the basis for a potentially very different photochemical behavior of GFP under femtosecond excitation compared to CW excitation conditions. Ultrafast spectroscopy, for separating the competing photoreactions of photoconversion and excited state proton transfer, is hampered, however, by the small quantum yield for the irreversible photoreaction.

In our contribution, we compensate for the drawback of a low yield of photoproduct by a new spectroscopic method—accumulative spectroscopy—that we have recently developed (16). Whereas conventional pump-probe spectroscopy is performed with a continuous exchange of the sample with fresh material, in our technique, photoproducts (i.e., in this case the photoconverted protein) are accumulated over a series of pulse sequences. In this way, pump-probe transients can be measured even when the photochemical conversion efficiency is extremely low. Here we examine the GFP mutant T203V. This mutant is particularly appropriate for investigating photoconversion due to the preponderance of RH (Fig. 2) and the detailed knowledge about its fluorescence dynamics (11,17–19).

It will be shown by accumulative studies that transitions to a higher excited state are the major contribution to photoconversion upon pulsed excitation. Time-resolved two-color accumulative pump-probe spectroscopy is then performed, yielding the timescales of the initial steps of photoconversion. This provides further evidence for the importance of the transient RH* species in the photoconversion process.

MATERIALS AND METHODS

GFP mutant T203V was kindly provided by J. Wiehler, Gene Center, Munich, Germany. We used the undiluted sample, which was buffered to physiological conditions with an optical density (OD) of ≈10/cm at λ_{max}.

The general experimental method used for product detection used here has been described elsewhere (16). In these accumulative experiments (Fig. 3), a sequence of pulses from a femtosecond laser interacts with a small sample volume of GFP solution inside a glass capillary (Hellma, Müllheim, Germany) for a time of 3 s (controlled by a beam shutter). Thus, only permanent photoproducts—in this case, the photoconverted form of GFP, R_{pc}^-—are accumulated in the capillary interaction volume and the product yield is measured by optical absorption after the exposure.

The laser system used for these experiments consists of a home-built Ti:sapphire oscillator and a regenerative amplifier (Quantronix, East

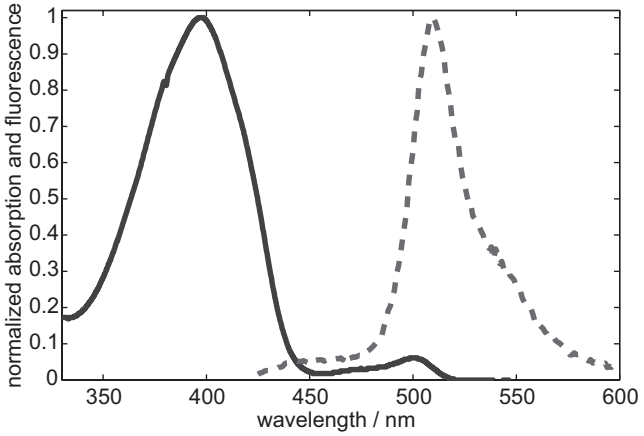

FIGURE 2 Normalized absorption (*solid line*) and fluorescence (*dashed line*) spectra of the T203V mutant of GFP used in this work.

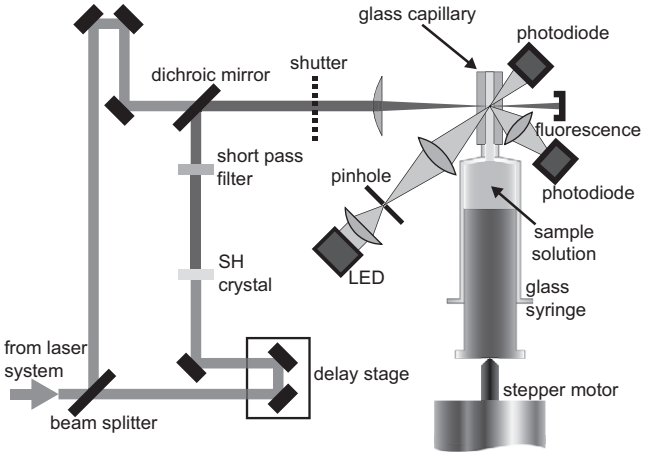

FIGURE 3 Schematics of the experimental setup.

Setauket, NY) that generates pulses of 80-fs duration centered at ~800 nm at a repetition rate of 1 kHz. For the power study of fluorescence and photoconversion these pulses were attenuated by a variable filter wheel (Thorlabs, Newton, NJ) and their energy was measured with a small beam pick-off and a photodiode (Laser Components, Olching, Germany) before sending them to the sample. The fluorescence was collected by a microscope objective above the capillary, passed through a green interference filter, and its intensity was measured with another photodiode. Due to our laser repetition rate of 1 kHz the RH species completes a full photocycle of excitation, excited state proton transfer, fluorescence, and reprotonation between two consecutive pulses.

For the time-resolved two-color experiment the beam from the laser system was split into two arms (Fig. 3); the pulses in one arm were time-delayed and frequency-doubled in a 100-μm β-Barium-Borate crystal. A short-pass filter (BG39, Schott) eliminates the remaining fundamental light and a dichroic mirror (Laser Components) recombines the 400-nm pulses with the 800-nm pulses from the other arm collinearly. In addition, the pulse energy in each arm can be adjusted independently with two variable attenuator wheels (not drawn). The diameter of the 800-nm beam was adjusted with an aperture so that, after focusing, both beams had a diameter of $\approx$200 μm inside the capillary. To ensure the best possible time resolution and to avoid timing offsets we compressed the pulses and placed a slab of glass, which was as thick as the wall of the capillary holding the sample, into the common beam path and performed a cross-correlation of the 400- and 800-nm pulses in a sum-frequency mixing crystal. This procedure reveals a time-resolution of 165 fs.

The measurement sequence consists of the following steps: First the stepper motor pushes the glass syringe forward to bring a fresh sample volume into the interaction region. The pulse configuration is adjusted, i.e., the time delay between 400- and 800-nm pulses is adjusted (in the pump-repump experiments) or the energy of the pulses is changed (in the power study). Then the shutter is opened and the exposure time starts. During the first few laser shots that hit the sample, we collect the fluorescence signal. In all the experiments shown here, we used an exposure time of 3 s, thus roughly 3000 pulses irradiated the pump volume. After closing the shutter again, the absorption of the pump volume at 504 nm is obtained through a measurement of the transmitted intensity of a light-emitting diode. We use a 100-μm pinhole in front of the light-emitting diode and image this pinhole into the pump volume. This defines the probe volume, which is slightly smaller than the pump volume. Thereafter, the cycle starts again with a fresh sample volume. This sequence is computer-controlled and can be repeated automatically many times. Due to the small cross section of the glass capillary (250 μm $\times$ 250 μm), the smallest amounts of sample volume are sufficient for these types of measurements. A typical experiment, e.g., the one from Fig. 6, uses only ~50 μL of sample solution.

The concentrations of the different molecular species RH, R^-_{eq}, and R^-_{pc} evolve over the exposure time according to the efficiency of the irradiating laser pulses. However, since the accumulation of the photoproducts happens on a timescale of a few seconds, one has to take the diffusion of all reactants in and out of the laser interaction volume and the probed volume into account. The accumulation is therefore nonlinear in exposure time and in the efficiency η of the laser pulses. (The quantity η can be regarded as the product of the quantum efficiency Φ and the probability for excitation. However, especially with possible multiphoton excitations, the probability for excitation is not easy to determine. For studies of the efficiency of a process such as photoconversion, for given conditions as in this article, it is sufficient to consider the efficiency η only.) Without compensating for the nonlinearities in the accumulation process, and taking only the measured absorption after exposure, this would lead to distorted results and interpretations of the data. However, a correction for this diffusion can be done analogous to the procedure described in Langhojer et al. (16): a simple mathematical model for the accumulation and diffusion has to be found; a calibration measurement is performed; the model is fit to that data; and finally, the obtained calibration is applied to correct any other experimental data to gain the efficiency η (i.e., the fraction of all molecules in the laser-exposed volume that undergoes photoconversion).

Here, basically, three species have to be considered in the accumulation process: RH, R^-_{eq}, and R^-_{pc}. The femtosecond laser pulses at 400 nm or 800 nm are only resonant with the one-photon or two-photon absorption of the predominant RH species of T203V GFP. Since photoconversion leads to R^-_{pc} and the optical absorption properties of R^-_{eq} are equal to those of R^-_{pc} (4), we can restrict ourselves to the two spectroscopically distinguishable species A and B with absorption maxima at 397 nm and 500 nm, respectively (Fig. 2). The geometry of pump and probe volumes, including the constants describing the dynamics during exposure, is shown schematically (Fig. 4, *inset*). Using a simple exchange rate d_{pu} between the pump volume and the bulk sample solution, one can attain the following differential equations to describe the concentration dynamics of A and B during the exposure ($0 \le t \le \tau$, the total exposure time is τ):

$$\dot{A}_{pu}(t) = -\eta A_{pu}(t) + d_{pu}\big(A_0 - A_{pu}(t)\big), \quad (1)$$

$$\dot{B}_{pu}(t) = \eta A_{pu}(t) + d_{pu}\big(B_0 - B_{pu}(t)\big). \quad (2)$$

A_{pu} and B_{pu} are the concentrations of A and B in the pump volume. The initial conditions are dictated by the homogeneous concentrations of both A and B throughout the capillary:

$$A_{pu}(0) = A_{pr}(0) = A_0, \quad (3)$$

$$B_{pu}(0) = B_{pr}(0) = B_0. \quad (4)$$

For determining the effects of the pump laser on the sample in the pump volume, the probe light is focused on a volume smaller than the pump volume. During the exposure time τ, the concentrations in this probe volume, A_{pr} and B_{pr}, develop just like the concentrations in the bigger pump volume:

$$A_{pr}(t) \equiv A_{pu}(t), \quad (5)$$

$$B_{pr}(t) \equiv B_{pu}(t). \quad (6)$$

To characterize the diffusion in the calibration experiment independent of the molecular dynamics, we introduce an additional waiting time T after the end of the exposure time τ and before measuring the absorption of B ($t > \tau$, $T = t - \tau$). Then B evolves according to

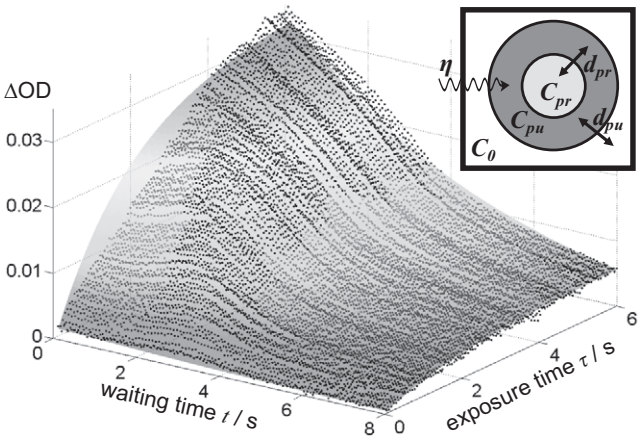

FIGURE 4 Calibration scan of the accumulation setup. Data shown as dots, best fit to model function shown as shaded surface. (*Inset*) Concentrations C_i in different volumes i defined by beam geometry with rates for diffusion d_i and product accumulation η (see text).

$$\dot{B}_{\mathrm{pu}}(T) = d_{\mathrm{pu}}\big(B_0 - B_{\mathrm{pu}}(T)\big) - d_{\mathrm{pr}}\big(B_{\mathrm{pu}}(T) - B_{\mathrm{pr}}(T)\big), \quad (7)$$

$$\dot{B}_{\mathrm{pr}}(T) = d_{\mathrm{pr}}\big(B_{\mathrm{pu}}(T) - B_{\mathrm{pr}}(T)\big). \quad (8)$$

The constant d_{pr} is the diffusion exchange rate between the pump and probe volume, analogous to d_{pu} (Fig. 4, *inset*).

The conditions for joining Eqs. 7–8 with Eqs. 1 and 2 are

$$B_{\mathrm{pu}}(t = \tau) = B_{\mathrm{pu}}(T = 0) \quad (9)$$

and

$$B_{\mathrm{pr}}(t = \tau) = B_{\mathrm{pr}}(T = 0). \quad (10)$$

The differential equations (1–6) were solved with the Mathematica software package (Wolfram Research, Champaign, IL) and the solutions for times $0 < t < \tau$ during the exposure to the femtosecond pulses are

$$A_{\mathrm{pu}}(t) = A_{\mathrm{pr}}(t) = \frac{A_0}{d_{\mathrm{pu}} + \eta}\big(d_{pu} + \eta \mathrm{e}^{-(d_{\mathrm{pu}} + \eta)t}\big), \quad (11)$$

$$B_{\mathrm{pu}}(t) = B_{\mathrm{pr}}(t) = \frac{A_0\eta}{d_{\mathrm{pu}} + \eta}\big(1 - \mathrm{e}^{-(d_{\mathrm{pu}} + \eta)t}\big) + B_0. \quad (12)$$

The solutions for Eqs. 7–10 for nonzero waiting times T after the exposure ($T \equiv t - \tau$, $t > \tau$) are

$$B_{\mathrm{pu}}(\tau, T) = \frac{1}{2s\big(d_{\mathrm{pu}} + \eta\big)} \times \exp\left[-\frac{3}{2}\big(d_{\mathrm{pu}} + 2d_{\mathrm{pr}}\big)T - \frac{1}{2}sT - \big(d_{\mathrm{pu}} + \eta\big)\,\tau\right] \times \Big\{A_0\eta\exp\big[\big(d_{\mathrm{pu}} + 2d_{\mathrm{pr}}\big)T\big] \times \big(\exp\big[\big(d_{\mathrm{pu}} + \eta\big)\tau\big] - 1\big) \times \big(d_{\mathrm{pu}} + \big(s - d_{\mathrm{pu}}\big)\exp[sT] + 2d_{\mathrm{pr}}(\exp[sT] - 1) + s\big) + 2B_0 s\big(d_{\mathrm{pu}} + \eta\big)\exp\left[3d_{\mathrm{pr}}T + \frac{3}{2}d_{\mathrm{pu}}T + \frac{1}{2}sT + \big(d_{\mathrm{pu}} + \eta\big)\tau\right]\Big\} \quad (13)$$

and

$$B_{\mathrm{pr}}(\tau, T) = \frac{1}{2s\big(d_{\mathrm{pu}} + \eta\big)} \times \exp\left[-\frac{3}{2}\big(d_{\mathrm{pu}} + 2d_{\mathrm{pr}}\big)T - \frac{1}{2}sT - \big(d_{\mathrm{pu}} + \eta\big)\tau\right] \times \Big\{A_0\eta\exp\big[\big(d_{\mathrm{pu}} + 2d_{\mathrm{pr}}\big)T\big] \times \big(\exp\big[\big(d_{\mathrm{pu}} + \eta\big)\tau\big] - 1\big) \times \big(-d_{\mathrm{pu}} + \big(s + d_{\mathrm{pu}}\big)\exp[sT] + 2d_{\mathrm{pr}}(\exp[sT] - 1) + s\big) + 2B_0 s\big(d_{\mathrm{pu}} + \eta\big)\exp\left[3d_{\mathrm{pr}}T + \frac{3}{2}d_{\mathrm{pu}}T + \frac{1}{2}sT + \big(d_{\mathrm{pr}} + \eta\big)\tau\right]\Big\} \quad (14)$$

with

$$s = \sqrt{d_{\mathrm{pu}}^2 + 4d_{\mathrm{pr}}^2}. \quad (15)$$

So far, the discussion has dealt with the total number N of molecules of the A and B form in the pump and in the probe volume. Absorbance (or optical density) OD is defined via $I/I_0 = 10^{-\mathrm{OD}}$ with the intensities I after, and I_0 before, passing through the sample. To make the transition to absorbance OD (the signal from the experiment), we consider the proportionality

$$\mathrm{OD} \propto \varepsilon N. \quad (16)$$

Thus, substituting

$$A \rightarrow \mathrm{OD}_{\mathrm{A}}/\varepsilon_{\mathrm{A}} \quad (17)$$

$$B \rightarrow \mathrm{OD}_{\mathrm{B}}/\varepsilon_{\mathrm{B}} \quad (18)$$

and defining

$$c \equiv \frac{\varepsilon_{\mathrm{B}}}{\varepsilon_{\mathrm{A}}} \quad (19)$$

as the ratio of the absorptivities of the two forms, we can write

$$\Delta\mathrm{OD}_{\mathrm{B}}(\tau, T) = \varepsilon_{\mathrm{B}}B_{\mathrm{pr}}(\tau, T) - \mathrm{OD}_{\mathrm{B0}} = \frac{1}{2s\big(d_{\mathrm{pu}} + \eta\big)}\exp\left[-\frac{3}{2}\big(d_{\mathrm{pu}} + 2d_{\mathrm{pr}}\big)T - \frac{1}{2}sT - \big(d_{\mathrm{pu}} + \eta\big)\tau\right] \times \Big\{c\mathrm{OD}_{\mathrm{A0}}\eta\exp\big[\big(d_{\mathrm{pu}} + 2d_{\mathrm{pr}}\big)T\big]\big(\exp\big[\big(d_{\mathrm{pu}} + \eta\big)\tau\big] - 1\big) \times \big(-d_{\mathrm{pu}} + \big(s + d_{\mathrm{pu}}\big)\exp[sT] + 2d_{\mathrm{pr}}(\exp[sT] - 1) + s\big) + 2\mathrm{OD}_{\mathrm{B0}}s\big(d_{\mathrm{pu}} + \eta\big)\exp\left[3d_{\mathrm{pr}}T + \frac{3}{2}d_{\mathrm{pu}}T + \frac{1}{2}sT + \big(d_{\mathrm{pr}} + \eta\big)\tau\right]\Big\} - \mathrm{OD}_{\mathrm{B0}}. \quad (20)$$

Only the absorbance in the probe volume is of interest; therefore, we simply write ΔOD_B instead of $\Delta OD_{B,pr}$ to denote the change of absorbance measured at 504 nm in the experiment. We used the numeric values of the absorption cross sections of A and B from Wiehler et al. (11). The initial absorbances $OD_A(t \leq 0)$ and $OD_B(t \leq 0)$ of the unexposed sample volume were gained in an independent measurement. Thus, the function $\Delta OD_B(\tau, T)$ has the three remaining free parameters d_{pu}, d_{pr}, and η. Whereas the latter depends on the properties of the applied laser pulses that induce photoconversion, and thus is the objective of the actual pump-repump and power study experiments, the first two parameters only depend on the measurement geometry and the diffusion properties of GFP in the buffer solution and are therefore constant for all experiments studying different femtosecond pulse configurations.

To retrieve these diffusion rates we fit the model function Eq. 20 to the calibration data. This data is gained by scanning the exposure time between 0 and 6 s and taking the absorbance measurement after an additional waiting time that is varied between 0 and 8 s. Fig. 4 shows the data together with a best fit obtained from a least-squares optimization; the best parameters are $d_{pu} = 0.487$/s, $d_{pr} = 1.86$/s, and $\eta = 4.06 \times 10^{-5}$/pulse. We used the diffusion calibration for all experiments presented in this article by taking the obtained measurement data ΔOD_B as a function of pulse configuration (e.g., pump-repump delay time) and solving the fit model for the efficiency η numerically for each data point. This calibration is a nonlinear correction to the absorbance data and results in the diffusion-corrected efficiency of a certain pulse delay or a certain pulse energy for the time-resolved 400-nm plus 800-nm experiment and the power study, respectively. For stable photoproducts one thus obtains the same information with the accumulative method as with a conventional experiment, but with greatly enhanced sensitivity; differences in conversion efficiencies of $\Delta\eta = 2.3 \times 10^{-7}$ per pulse can be detected routinely. This sensitivity was determined from the standard deviation of the data points for $\Delta t < 0$ in Fig. 6. The change in η corresponds to a change in absorbance of $\Delta OD \approx 10^{-7}$ per pulse.

RESULTS AND DISCUSSION

We focus on photoconversion starting from the neutral ground state RH, which is the predominant species of the T203V mutant in thermal equilibrium (17) (Fig. 2). The accumulative method described in Materials and Methods is the basis for these experiments and allows us to detect even extremely small photoconversion efficiencies. First we conduct a power study of the photoinduced reaction. Although this is, in general, a rather simple experiment, to our knowledge it has not been performed yet on the efficiency of photoconversion of GFP, perhaps due to the low conversion efficiency in conventional flow-cell geometries. The accumulation setup, in contrast, facilitates an easy automated measurement with high sensitivity, where many data points can be taken with different sample volumes, while not imposing any special restrictions or demands on the sample concentration or the laser peak power. The results of such a power study using 800-nm laser pulses for excitation are shown in Fig. 5; both the fluorescence (Fig. 5 *a*) and the photoconversion (Fig. 5 *b*) were measured simultaneously. For interpretation, it should be considered that TPA microscopy with GFP as fluorescent marker is a common technique and exploits the fact that GFP (in its RH form) has a relatively strong TPA at ~800 nm (20,21). One therefore expects a proportionality of the fluorescence yield to the squared intensity of the pulses (or pulse energy, since the duration and beam

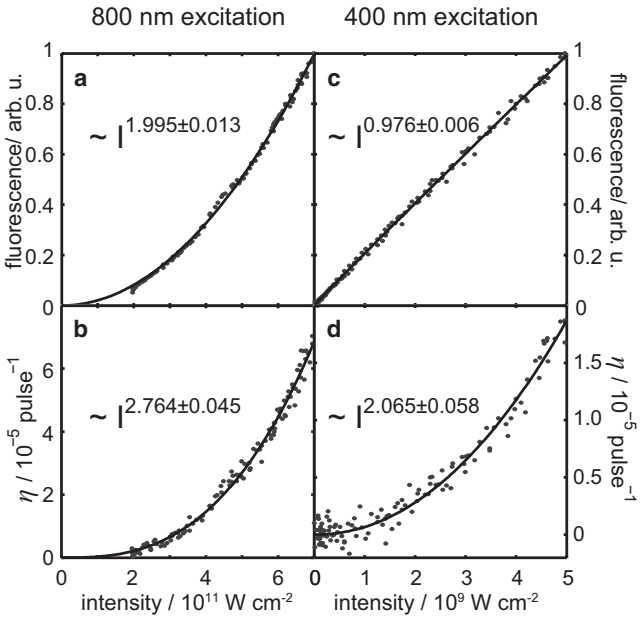

FIGURE 5 Power studies: (*a*) Fluorescence upon excitation with 800-nm pulses. (*b*) Photoconversion efficiency upon excitation with 800-nm pulses. (*c*) Fluorescence upon excitation with 400-nm pulses. (*d*) Photoconversion efficiency upon excitation with 400-nm pulses. The abscissas of all plots (*a–d*) represent the peak intensities in the sample.

profile are not altered). The best fit of the function $f = \alpha I^{\beta}$ to the data (Fig. 5 *a*, *solid line*) indeed reveals a quadratic dependence of the fluorescence on the excitation intensity. Moreover, even at the higher power levels we see no saturation effects. This confirms that the green fluorescence purely results from TPA of RH at 800 nm leading to RH* and subsequent excited state proton transfer.

For the photoconversion, on the other hand, the situation is more complex. In the original experiments, where photoconversion of a GFP variant (PA-GFP) was introduced as a means to mark structures in a cell and track them under a microscope, high levels of CW light, resonant with the RH → RH* transition, were used to trigger photoconversion (3). However, the nature of the reactive state remained unclear. Does photoconversion occur via TPA of RH into RH* as has been shown for a GFP variant (22)?

In our highly sensitive accumulative study we determined an exponent of the power dependence of 2.76 (Fig. 5 *b*). Here, the diffusion calibration has already been applied as described in Materials and Methods. This is significantly higher than what one would expect if photoconversion occurred from the same initial excited state RH* as fluorescence. Our data instead suggests that an efficient photoconversion can only be induced by absorption of at least three 800-nm photons leading to a higher excited state RH**, and that photoconversion predominantly starts from this RH** state rather than from RH*, which is the excited state of the regular fluorescence photocycle of GFP.

This conclusion is further supported by data taken with 400-nm instead of 800-nm excitation pulses. The

fluorescence (Fig. 5 *c*) shows a linear dependence on the excitation intensity, as expected. However, the dependence of photoconversion on the excitation intensity (Fig. 5 *d*) is ≈ 2, indicating that more than one photon is needed to induce photoconversion efficiently, and that excitation to a higher excited state is needed for photoconversion. Two 400-nm photons most likely excite a state that is higher-lying than RH** and can either lead to decarboxylation itself or undergo a fast conversion to the reactive RH**. The evidence for a consecutive TPA being responsible for the photoconversion of another autofluorescent protein, DsRed, reported by Habuchi et al. (23) corroborates our interpretation of this data. In a study of fluorescence dynamics of superfolder GFP upon TPA with 975 nm, Cotlet et al. (24) suggest that the photoconversion, which they detect indirectly via fluorescence lifetime of single molecules, is due to a 2+1 photon absorption. (Note that we do not exclude the possibility of photoconversion from R_I^-, but under our conditions any resulting linear component of the power dependence is concealed under the vastly greater nonlinear component because of excitation into RH**.)

We did not perform any experiments using UV excitation; however, this has been reported to be a very efficient way of inducing photoconversion (e.g., with $\lambda = 254$ nm in (15)). Presumably, wavelengths of ~267 nm, corresponding to three 800-nm photons, access RH** directly and are therefore efficient at photoconverting the RH species.

Although photoconversion must occur from the higher-lying RH**, RH* is a resonant intermediate state when exciting with either wavelength, 400 nm or 800 nm. It is an interesting question as to what role this state plays in the photoconversion, and what the dynamics of the RH* → RH** step of photoconversion might be. The experiments with 800- or 400-nm pulses shown in Fig. 5 require a molecule to absorb all photons from one pulse, and hence no time resolution is achieved. Aiming at separating the excitation to the photoconverting form into excitation to RH* and subsequent excitation to RH**, we employ a two-color experiment where a 400-nm pulse excites the GFP molecules and an 800-nm pulse, delayed by time t, induces photoconversion.

Fig. 6 shows the results of such an experiment. To avoid contributions due to one color only, the individual beam intensities were adjusted so that each of them only induces a small amount of photoconversion, 3 mOD absorbance change for the 800-nm and 6 mOD for the 400-nm beam, while the maximum photoconversion signal arising from both pulses together at $\sim t = 0$ was 22 mOD. In Fig. 6, the diffusion calibration has been applied as discussed in Materials and Methods. As a result, the photoconversion efficiency η is obtained. The value η describes the fraction of molecules in the interaction volume that are converted with a single 400-nm, 800-nm two-pulse sequence. The maximum photoconversion efficiency is $\eta = 3.4 \times 10^{-5}$ for $t \approx 0$, which represents an enhancement of a factor of 2.4 over the photoconversion efficiency yielded with the wrong time ordering of the excitation pulses (i.e., 800 nm first, $t < 0$). This clearly shows that there is a cooperative part to the photoconversion, requiring an interaction with the 400-nm pulse first and then another interaction with the 800-nm pulse. Therefore, we can say that the photoconversion can more easily be achieved (i.e., with less overall pulse energy) when first exciting to RH* and then exciting to the reactive RH**.

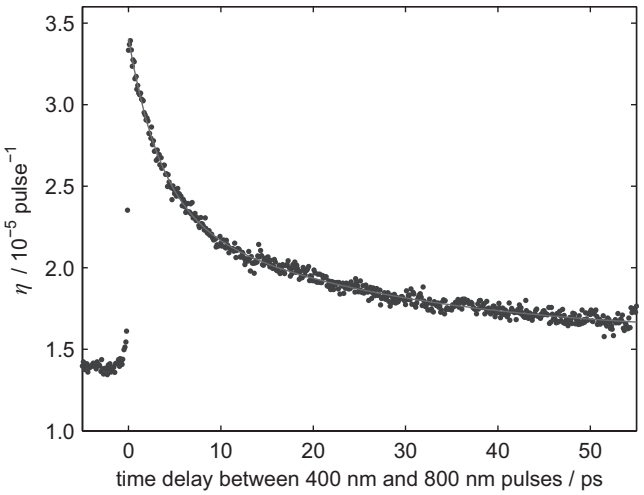

FIGURE 6 Time-resolved two-color experiment on photoconversion. After initial excitation of RH to RH* with a 400-nm pulse, a 800-nm pulse induces photoconversion, and the diffusion-corrected conversion efficiency (for a single laser pulse sequence) is shown as a function of pump-repump time delay. The constant offset at negative time delays is due to the photoconversion caused by the single 800- and 400-nm pulses.

By scanning the time delay of the two pulses, one can determine how efficient the excitation to RH** is a certain time after the initial excitation to RH*. Fitting a biexponential function $A_0 + A_1 \exp(-t/\tau_1) + A_2 \exp(-t/\tau_2)$ to the data for $t > 0$ yields time constants of $\tau_1 = (3.46 \pm 0.14)$ ps and $\tau_2 = (24.2 \pm 1.7)$ ps, with amplitudes of $A_0 = (1.585 \pm 0.015) \times 10^{-5}$, $A_1 = (1.027 \pm 0.027) \times 10^{-5}$, and $A_2 = (0.793 \pm 0.018) \times 10^{-5}$. If the noncooperative background of 1.4×10^{-5} is subtracted, the relative amplitudes ensue as $\tilde{A}_0 = 9.2\%$, $\tilde{A}_1 = 51.3\%$, and $\tilde{A}_2 = 39.5\%$.

Kummer et al. (17) measured the fluorescence decay of the protonated RH* form at 450 nm—i.e., the depopulation of RH* of the T203V mutant—with a time resolution of 6 ps, and found time constants of 5.4 ps and 17 ps to be the predominant contribution to the dynamics, with similar relative amplitudes to the amplitudes we found in the photoconversion experiment. These dynamics of fluorescence relaxation from the RH* state are the same within the experimental accuracy as the dynamics we find for excitation of the reactive RH** state from RH*. The deviation of Kummer's time constant of 5.4 ps from our time constant of 3.46 ps can likely be attributed to the low time resolution of 6 ps in their experiment (17). They also found contributions on longer timescales up to 400 ps adding up to a relative amplitude of $\approx 16\%$. However, the scanning range of our experiments

was limited to 55 ps and the small constant contribution of $\tilde{A}_0 = 9.2\%$ is most likely due to those slow contributions. Therefore, we argue that the excitation to the reactive RH** can only occur close to the Franck-Condon region that was accessed in the initial RH* excitation step. It is not likely that a later, relaxed species like R_I^-* is excited to the reactive state, because in that case, the transient in Fig. 6 would look like a step function, or even exhibit a rise of some picoseconds duration, due to the formation of the relaxed forms of GFP in the excited state. Instead, we observe that the timescales and amplitudes correspond to those for depopulation of the initially excited RH*.

CONCLUSIONS

Here, we have presented a study on the photoconversion of T203V GFP under femtosecond irradiation starting from the protonated species of the chromophore. By means of power studies in a novel accumulative setup with a sensitivity of $\Delta OD \approx 10^{-7}$, the photoconversion process was found to be largely governed by an initial excitation to a higher excited state of the chromophore RH**. From there, photoconversion is much more efficient than from the first excited state RH*. This supports earlier suggestions that the decarboxylation reaction of the Glu^{222} rest follows a Kolbe-type mechanism (15), because a higher excited state generally has a higher oxidative potential. To further investigate the role of RH* in the subsequent excitation to the reactive RH** state, we used a time-resolved two-color experiment where a 400-nm pulse excites RH to RH* and a time-delayed 800-nm pulse excites RH* to RH**. The probability of the latter process decreases with time constants very similar to those for the depopulation of RH* previously reported in the literature (17). Thus, with one 800-nm photon, the RH** state can only be reached from the region of the RH* potential energy surface where the initial excitation occurred and, due to the excited state dynamics, RH** can only be reached a few picoseconds after the initial excitation.

On the other hand, photoactivation under long pulse or CW excitation conditions as it has been exploited, for instance, by Patterson and Lippincott-Schwartz (3) is unlikely to occur via TPA due to the orders-of-magnitude lower intensities in those experiments. It rather seems likely that under those conditions the long-living R_I^-* state, which is created after excited state proton transfer, is responsible for photoconversion with a fairly low efficiency. This, however, can yield significant amounts of R_{pc}^- through prolonged (quasi-)CW irradiation (19,25).

In contrast, the findings of this study are particularly interesting, with respect to the use of GFP in TPA microscopy, because the high intensity levels of a typical setup using a femtosecond oscillator with tight focusing ($\approx 1\ \mu m$) are comparable with the intensity levels of our experiments with an amplified laser system and loose focusing. When using 800-nm pulses in a microscopy experiment, the process of ground-state absorption and subsequent excited-state absorption from RH* can be regarded as a resonance-enhanced multiphoton absorption; thus, there will always be some photoconversion in microscopy experiments, decreasing the fluorescence signal from 800 nm TPA over time, and also changing the fluorescence lifetimes (19,24).

We thank J. Wiehler (Gene Center, Munich, Germany) for the GFP sample.

This work was supported by the Emmy Noether Program of the German Science Foundation.

REFERENCES

1. Willig, K. I., R. R. Kellner, R. Medda, B. Hein, S. Jakobs, et al. 2006. Nanoscale resolution in GFP-based microscopy. *Nat. Methods*. 3: 721–723.
2. Betzig, E., G. H. Patterson, R. Sougrat, O. W. Lindwasser, S. Olenych, et al. 2006. Imaging intracellular fluorescent proteins at nanometer resolution. *Science*. 313:1642–1645.
3. Patterson, G. H., and J. Lippincott-Schwartz. 2002. A photoactivatable GFP for selective photolabeling of proteins and cells. *Science*. 297:1873–1877.
4. van Thor, J. J., T. Gensch, K. J. Hellingwerf, and L. N. Johnson. 2002. Phototransformation of green fluorescent protein with UV and visible light leads to decarboxylation of glutamate 222. *Nat. Struct. Biol.* 9:37–41.
5. Chalfie, M., Y. Tu, G. Euskirchen, W. Ward, and D. Prasher. 1994. Green fluorescent protein as a marker for gene expression. *Science*. 263:802–805.
6. Chattoraj, M., B. A. King, G. U. Bublitz, and S. G. Boxer. 1996. Ultrafast excited state dynamics in green fluorescent protein: multiple states and proton transfer. *Proc. Natl. Acad. Sci. USA*. 93:8362–8367.
7. Winkler, K., J. Lindner, V. Subramaniam, T. M. Jovin, and P. Vöhringer. 2002. Ultrafast dynamics in the excited state of green fluorescent protein (wt) studied by frequency-resolved femtosecond pump-probe spectroscopy. *Phys. Chem. Chem. Phys*. 4:1072–1081.
8. Lossau, H., A. Kummer, R. Heinecke, F. Pollinger-Dammer, C. Kompa, et al. 1996. Time-resolved spectroscopy of wild-type and mutant green fluorescent proteins reveals excited state deprotonation consistent with fluorophore-protein interactions. *Chem. Phys*. 213:1–16.
9. Stoner-Ma, D., A. Jaye, P. Matousek, M. Towrie, S. Meech, et al. 2005. Observation of excited-state proton transfer in green fluorescent protein using ultrafast vibrational spectroscopy. *J. Am. Chem. Soc*. 127:2864–2865.
10. Kennis, J. T. M., D. S. Larsen, I. H. M. van Stokkum, M. Vengris, J. J. van Thor, et al. 2004. Uncovering the hidden ground state of green fluorescent protein. *Proc. Natl. Acad. Sci. USA*. 101:17988–17993.
11. Wiehler, J., G. Jung, C. Seebacher, A. Zumbusch, and B. Steipe. 2003. Mutagenic stabilization of the photocycle intermediate of green fluorescent protein (GFP). *Chem. Bio. Chem*. 4:1164–1171.
12. van Thor, J., G. Zanetti, K. Ronayne, and M. Towrie. 2005. Structural events in the photocycle of green fluorescent protein. *J. Phys. Chem. B*. 109:16099–16108.
13. van Thor, J. J., G. Y. Georgiev, M. Towrie, and J. T. Sage. 2005. Ultrafast and low barrier motions in the photoreactions of the green fluorescent protein. *J. Biol. Chem*. 280:33652–33659.
14. van Thor, J. J., and J. T. Sage. 2006. Charge transfer in green fluorescent protein. *Photochem. Photobiol. Sci*. 5:597–602.
15. Bell, A., D. Stoner-Ma, R. Wachter, and P. Tonge. 2003. Light-driven decarboxylation of wild-type green fluorescent protein. *J. Am. Chem. Soc*. 125:6919–6926.
16. Langhojer, F., F. Dimler, G. Jung, and T. Brixner. 2007. Product accumulation for ultrasensitive femtochemistry. *Opt. Lett*. 32:3346–3348.

17. Kummer, A., J. Wiehler, H. Rehaber, C. Kompa, B. Steipe, et al. 2000. Effects of threonine 203 replacements on excited-state dynamics and fluorescence properties of the green fluorescent protein (GFP). *J. Phys. Chem. B*. 104:4791–4798.

18. Jung, G., J. Wiehler, and A. Zumbusch. 2005. The photophysics of green fluorescent protein: influence of the key amino acids at positions 65, 203, and 222. *Biophys. J*. 88:1932–1947.

19. Jung, G., M. Werner, and M. Schneider. 2008. Efficient photoconversion distorts the fluorescence lifetime of GFP in confocal microscopy: a model kinetic study on mutant $Thr^{203}Val$. *Chem. Phys. Chem*. 9:1867–1874.

20. Xu, C., R. M. Williams, W. Zipfel, and W. W. Webb. 1996. Multiphoton excitation cross-sections of molecular fluorophores. *Bioimaging*. 4:198–207.

21. Volkmer, A., V. Subramaniam, D. J. S. Birch, and T. M. Jovin. 2000. One- and two-photon excited fluorescence lifetimes and anisotropy decays of green fluorescent proteins. *Biophys. J*. 78:1589–1598.

22. Schneider, M., S. Barozzi, I. Testa, M. Faretta, and A. Diaspro. 2005. Two-photon activation and excitation properties of PA-GFP in the 720–920-nm region. *Biophys. J*. 89:1346–1352.

23. Habuchi, S., M. Cotlet, T. Gensch, T. Bednarz, S. Haber-Pohlmeier, et al. 2005. Evidence for the isomerization and decarboxylation in the photoconversion of the red fluorescent protein DsRed. *J. Am. Chem. Soc*. 127:8977–8984.

24. Cotlet, M., P. M. Goodwin, G. S. Waldo, and J. H. Werner. 2006. A comparison of the fluorescence dynamics of single molecules of a green fluorescent protein: one- versus two-photon excitation. *Chem. Phys. Chem*. 7:250–260.

25. Testa, I., D. Mazza, S. Barozzi, M. Faretta, and A. Diaspro. 2007. Blue-light (488 nm)-irradiation-induced photoactivation of the photoactivatable green fluorescent protein. *Appl. Phys. Lett*. 91: 133902–133903.